Energy and vapor transfer in evaporation processes over saturated bare soil and water surface-lysimeter studies

Wanxin Li[1,2],Wenke Wang[1,2,*], Yuankai Yang[3], Xinyue Hou[1,2], Hongting Ha[1,2]

[1] School of Water and Environment, Chang'an University, P. R. China

[2] Key Laboratory of Subsurface Hydrology and Ecological Effects in Arid Region, Chang'an University, Ministry of Education, P. R. China

[3] Nukleare Entsorgung und Reaktorsicherheit (IEK-6), Forschungszentrum Jülich GmbH, Jülich, Germany

***Corresponding author:**

Present/permanent address: School of Water and Environment, Chang'an University, Yanta Road 126, 710054, Xi'an, Shaanxi, the People's Republic of China

Tel.: +86 29 82339291,

Mail address: wenkew@chd.edu.cn (W. Wang)

Abstract

Potential evaporation (PE) is a significant input in many hydrological numerical models for the estimation of actual evaporation. Evaporation from water (PE_w) is generally considered equivalent to evaporation from saturated bare soils (PE_s). The influences of the underlying surface on PE as well as the energy and vapor transfer in potential evaporation processes over different surfaces are rarely discussed. In this research, lysimeter experiments were set up to measure the diurnal cycles of evaporation from two saturated sandy soils and water at a high temporal resolution in the Guanzhong Basin, China. Evaporation from Class A Pan, meteorological variables and temperatures were also measured during the experiment. Observation results show that PE_s is ~12% higher than PE_w on a yearly scale. There were also some clear differences in diurnal and seasonal PE dynamics between saturated bare soils and water. In summer, PE_s is higher than PE_w at day but smaller at night, with the peak value of PE_w lagging ~4 hours behind PE_s.

These observed PE dynamics and energy transfer processes can be quantitative explained on the basis of a full analysis of the energy balance equation. A comprehensive description of the flux transfer processes showed that these differences in PE are governed by differences in available energy (including albedo and thermal properties) between soils and water. Moreover, the observed differences in PE and vapor transfer processes were reproduced and described by improving the vapor diffusion equation, with considering the influence of different surfaces and boundary layer thicknesses. It is found that dynamics in PE were mainly characterized by surface temperature, which further determined the vapor gradients between the evaporation surface and air flow. The results suggested that differences between PE_s and PE_w cannot be neglected in hydrological applications. This study can act as both an experimental and theoretical reference for estimating potential evaporation rates.

Keywords: saturated bare soil evaporation, water evaporation, lysimeter, energy balance, vapor diffusion

Abbreviations

PE potential evaporation

PE_s evaporation from saturated bare soils

PE_{fine} evaporation from saturated fine sand

PE_{coarse} evaporation from saturated coarse sand

PE_w evaporation from water surfaces

PE_{col} evaporation from water filled lysimeter column

PE_{pan} evaporation from water filled Class A Pan

1. Introduction

Evaporation from a surface with sufficient water supply is known as potential evaporation (PE). PE is an important variable considered in many disciplines and numerical models (hydrology, hydrogeology, agriculture, and land surface modelling) to estimate actual evaporation (E_a) from soil (Ben Neriah et al., 2014; Bormann, 2011; Han et al., 2014; Kirono et al., 2010) or from phreatic water (Zhidong et al., 1988). Although several definitions of PE have been proposed (J.-P. Lhomme, 1997), they generally fall within two categories according to the surface type. They are evaporation from saturated bare soils (PE_s) and evaporation from water surface (PE_w).

PE_s is close to the Stage I Evaporation (early stages of evaporation from saturated soils with an initially high and relatively constant rate). PE_s is considered to be driven by atmosphere forcings and soil properties (Allen et al., 2005; Eberbach et al., 2011). However, in those experiments which investigate how soil type affects PE_s, soil columns were only saturated initially. There remain limited quantitative studies on the influence of soil texture on evaporation rate under a constantly saturated soil. In fact, PE_s and PE_w, as well as the evaporation rate from pan (PE_{pan}) have all been used as PE to estimate actual evaporation rate in applications (Allen et al., 1989; Granger, 1989; Kirono et al., 2010; Lehmann & Or, 2013; J. P. Lhomme & Guilioni, 2010; L. Wang et al., 2021; Westra, 2009). While this simplification relies on several hypotheses, differences in PE over saturated textures and water have not been quantitatively explored, nor have these differences been compared with PE_{pan} based on measured results at a high temporal resolution.

PE is a highly dynamic process reflecting the interplay between atmospheric conditions (energy input related to meteorological elements) and flow process (vapor diffusion) (Lim et al., 2012, 2013, 2016; Shahraeeni et al., 2012). The energy transfer process over different evaporation surfaces can be expressed based on the energy balance equation (Hamdani et al., 2018; Lim et al., 2013). However, applications sometimes adopt a simplified flux term in the full-form energy balance equation. For example, since there are rarely measurements of total ground heat flux for soil G (or the heat storage variation for water N) at meteorological stations,

they are often ignored within daily calculations of PE or assumed to be a fraction of net radiation over a sub-daily scale (Allen et al., 2005). Since G and N must be considered over shorter periods, the dynamics of evaporation should be described by a comprehensive analysis of the energy balance, considering the influences of different surfaces on flux terms.

Vapor from saturated bare soil (water filled porous) and water is mainly transported by diffusion across the boundary layer above the evaporation surface (Bird et al., 1961; Haghighi et al., 2013; Lehmann & Or, 2013; Shahraeeni et al., 2012). Solutions based on diffusion transport (such as Fick's First Law of Diffusion) determine that evaporation rate is characterized by vapor concentration gradients between evaporation surface and the flowing air as well as the thickness of the boundary layer δ (Ben Neriah et al., 2014; Dalton, 1802; Haghighi & Or, 2013; Lehmann et al., 2018; Lehmann & Or, 2013; Lim et al., 2012; Schlünder, 1988). However, previous research (Haghighi et al., 2013) has determined that δ can be defined by velocity convections. There have been no previous comparisons of the differences in δ among saturated soil and water.

Energy transfer and vapor transfer are inter-dependent processes essential for characterizing evaporation dynamics. These two drivers are thought to be influenced by the properties of evaporation surfaces, and are regulated by various factors including available energy, vapor pressure, and climate elements. To the best of our knowledge, exploration of this two-component interpretation in evaporation process between saturated bare soils and water over sub-daily scale for semi-arid region is a research gap, thus should be addressed in detail.

The present study implemented a unique lysimeter experiment in which evaporation over saturated fine sand (PE_{fine}), coarse sand (PE_{coarse}), water in the lysimeter columns (PE_{col}) as well as water in the Class A Pan (PE_{pan}) were measured at a high temporal resolution in the Guanzhong Basin to investigate the following objectives:

1. Investigating the differences of total evaporation over one year as well as the differences of sub-daily transient evaporation in different seasons between saturated fine sand, coarse sand and water surfaces.
2. Characterizing the differences in PE from a fully analysis of the energy balance and the vapor transfer in evaporation processes.

3. Evaluating the PE-estimation methods for characterizing the variables regulating energy transfer and vapor transfer processes over saturated bare soils and water.

2 Materials and methods

2.1 Materials

2.1.1 Lysimeter columns

The lysimeter experiment was conducted at Chang'an University, Xi'an, Guanzhong Basin, China (Latitude: 34°28' N; Longitude: 108°93' E). The setup of the experiments is show in Figure 1.

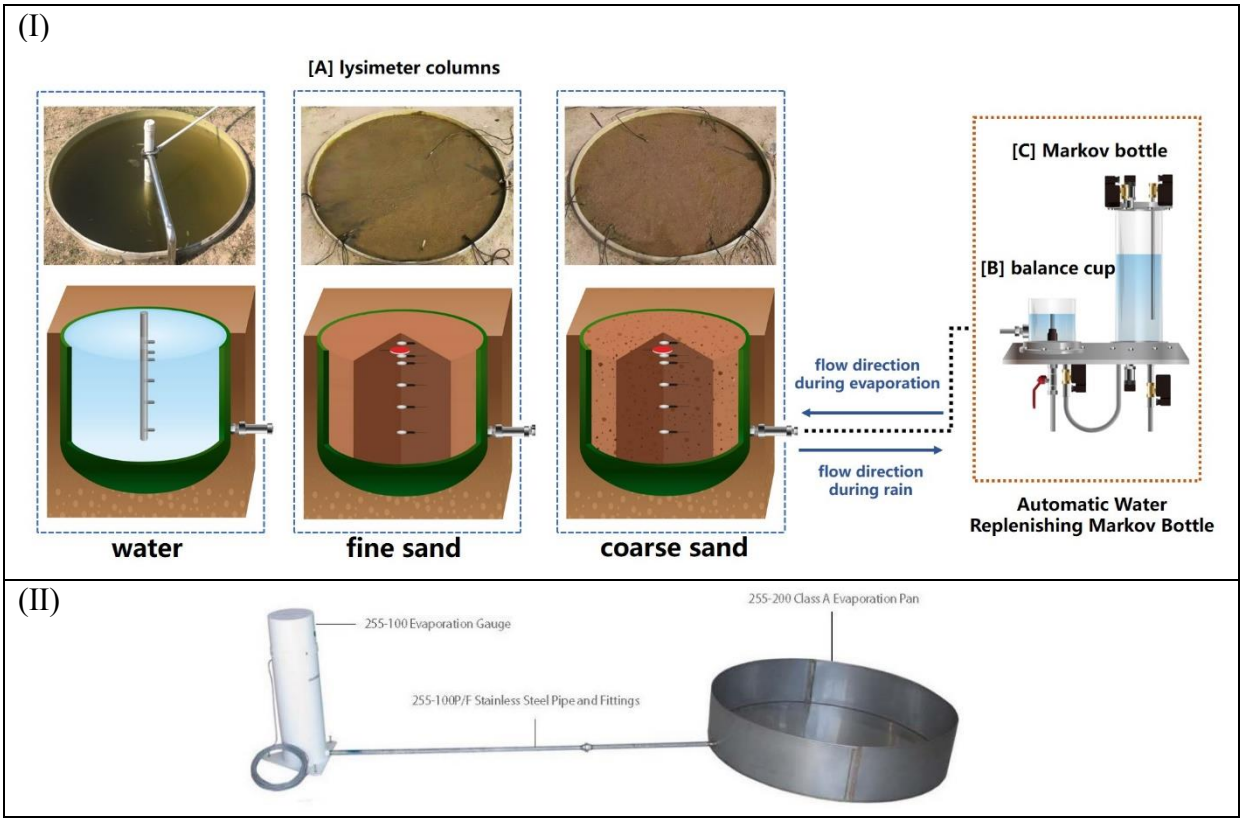

Figure 1: (I) Setup of the lysimeter experiment. (II)Setup of the Class A Pan.

Lysimeters allow to measure evaporation rates directly (Allen, Howell, et al., 1991; Allen, Pruitt, et al., 1991; Goss & Ehlers, 2010; Pütz et al., 2018). As Figure 1 (I) illustrates, lysimeter columns (area 1.0 m^2, depth 70cm) are filled with water and two different homogeneous soil textures. Evaporation rate from saturated soil textures (PE_s) and water (PE_w) were observed by the "Automatic Water Replenishing Markov Bottle" (installed in the basement). This Markov

Bottle based lysimeter device got a Utility Model Patent in 2014 (ZL2014200056418.x), and can provide reliable potential evaporation rate directly (Jensen et al., 2016; Truong, 2012; K. Wang & Dickinson, 2012).

The bottom of each column (A) was connected to a Markov Bottle (C) via the balance cup (B). The water table in the columns can be maintained at the soil and water surface so that potential evaporation rate equals to mass losses of water from the Markov Bottle to the lysimeter. In this experiment, a drop of the water level in the Markov Bottle of 94 cm coincides with an evaporation rate in the lysimeter column of 1 cm. The water level variation in the Markov Bottle were automatically measured using pressure sensors (MPM489, Microsensor).

Temperatures (for soil: MPS 6, for water: 1/3DIN) in the columns were observed at 3, 5, 10, 20, 30 and 50 cm depth. Heat flux G_0 (HFP01, Hukeflux Inc.) were observed at 5 cm depth in the soil column. Data are automatically recorded by the data logger (CR1000, Campbell Scientific Inc. USA) every 5 minutes.

2.1.2 Class A Pan evaporation and meteorological stations

As Figure 1 (II) illustrates, the Class A Pan (diameter 120.6 cm, depth 25 cm) was equipped with an evaporation gauge (255-100 Novalynx Analog Output Evaporation Gauge and 255-200 Novalynx Class A Evaporation Pan, Campbell Scientific Inc. USA). The pan evaporation rate can be measured directly by recording the water level variations. Temperature sensors were placed at the center of the pan (10 cm away from the bottom) to measure the bulk water temperature. Temperatures on water profile were measured at 3, 10 and 15cm depth below the surface.

The standard meteorological station is located in the southwestern part of the experimental site. Humidity-temperature sensors (083E-1-6, Met One Instrument, USA), air pressure sensor (Vaisala PTB110 Barometer-CS106, Campbell Scientific Inc. USA) and net radiometer (CNR4, Kipp&Zonen, Netherlands) were installed at 1.5 m above the ground. Wind speed sensors were located at 2 m and 10 m respectively. The measured data were automatically recorded every 5

minutes by CR-3000 (Campbell Scientific Inc. USA). The present study determined PE and other parameters at a 1-hour temporal resolution.

2.2 Methods and theory

2.2.1 Energy balance equation

The energy balance between an evaporation surface and the atmosphere can be expressed as:

$$\begin{aligned} R_{n,s} - G &= LE_s + H_s \\ R_{n,w} - N &= LE_w + H_w \end{aligned} \tag{1}$$

where R_n is the net radiative flux ($W \cdot m^{-2}$), G is the total ground heat flux ($W \cdot m^{-2}$), N is the variation in water heat storage ($W \cdot m^{-2}$), H is the convective energy exchanged between air and the evaporation surface ($W \cdot m^{-2}$), LE is the latent heat flux due to evaporation ($W \cdot m^{-2}$), and subscripts *s* and *w* refer to soil and water, respectively.

R_n includes net shortwave radiation (R_{ns}) and net longwave radiation (R_{nl}):

$$R_n = R_{ns} + R_{nl} = (1-\chi) \cdot R_{sd} + \varepsilon \cdot R_{ld} - R_{lu} \tag{2}$$

Net radiation is a critical input for estimating the evaporation rate (Han et al., 2014). In Equation (2), R_{sd} ($W \cdot m^{-2}$) and R_{ld} ($W \cdot m^{-2}$) represent measured downwards shortwave and downwards longwave radiation at the meteorological station, respectively and R_{lu} ($W \cdot m^{-2}$) is the outgoing longwave radiation emitted from the surface (Lawrence et al., 2019; Saito et al., 2006):

$$R_{lu} = \varepsilon \cdot \sigma \cdot (T + 273.14)^4 \tag{3}$$

where ε is the surface emissivity, σ is the Stefan-Boltzman constant ($=5.67\times10^{-8}\ Wm^{-2}K^{-4}$) and T (℃) is the surface temperature. The present study used temperatures measured at depths of 3 cm and 5 cm to estimate T using linear extrapolation. R_{ns} and R_{lu} represent the differences in albedo χ and surface temperature between soil and water, respectively.

For soil, G can be estimated as:

$$G = G_0 + \Delta S \tag{4}$$

Soil heat flux G_0 is measured using heat flux plates. The rate of soil heat storage ΔS above the heat flux plate is calculated as (Ochsner et al., 2007; Roxy et al., 2014):

$$\Delta S = \Delta z \cdot c_s \cdot \frac{(T_i - T_{i-1})}{\Delta t} \quad (5)$$

where soil temperature measured at 3 cm is used to estimate ΔS, T_i-T_{i-1} (K) is the temporal variation in temperature (where i represents time), Δz is the thickness of the layer (5 cm for soil), Δt is the time step, c_s (MJ/m^{3}K) is the volumetric heat capacity for saturated soil texture [Appendix, Equation (A2)], the rate of water heat storage N is calculated by Equation (5), and Δz is the depth of water in the column (Δz is 25 cm for water in Class A Pan evaporation, the present study divided the depth of the water column into 10-cm layers).

The sensible heat flux H can be estimated according to a resistance-type formulation (Cellier et al., 1996; Griend & Owe, 1994; Stewart et al., 1994):

$$H = \frac{\rho \cdot c_p \cdot (T - T_a)}{r_a} \quad (6)$$

where T_a is the air temperature, c_p is the specific heat of air, ρ (kg·m^{-3}) is the air density, and r_a (s·m^{-1}) is the aerodynamic resistance [given in the Appendix Equation (A3)].

The latent heat flux LE for evaporation can be estimated from the evaporation rate, where L is the latent heat of vaporization.

2.2.2 Vapor transfer equation

Vapor transfer from the evaporation surface to air E_{vapor} can be expressed based on Fick's First Law of Diffusion and the boundary layer theory (Lehmann et al., 2018; Lim et al., 2012):

$$E_{vapor} = \frac{M_w \cdot D_v \cdot \alpha}{R \cdot \rho_w} \cdot \frac{[e_s(T)/T - e_a(T_a)/T_a]}{\delta} \quad (7)$$

where M_w (= 0.018 kg·mol^{-1}) is the molecular mass of water, R (= 8.3 J·mol^{-1}·K^{-1}) is the ideal gas constant, ρ_w (= 1,000 kg·m^{-3}) is the water density, α is continuous water availability at the surface, for saturated texture α equals to the saturated content θ_s, for water α equals to 1. D_v (m^2·s^{-1}) is the diffusion coefficient for water vapor in air (Ben Neriah et al., 2014), e_s is the vapor pressure at the surface (Pa), which is assumed to be equivalent to the saturated vapor pressure at the surface temperature T, $e_a(T_a)$ is the actual vapor pressure of air at the reference

height, and $e_s(T)/T-e_a(T_a)/T_a$ represents the vapor pressure gradient between the surface and air (Δe).

According to the boundary layer theory, δ (mm) is the thickness of the boundary layer above the surface. Quantifying δ is difficult due to complex "mixed convection" between porous media, water, and the atmosphere, an alternative empirical calculation of δ is given as:

$$\delta = a \cdot U^{-0.5} \quad (8)$$

where δ is inversely proportional to the square root of the free-stream velocity U (Ben Neriah et al., 2014; Ghezzehei et al., 2004; Haghighi et al., 2013; Shahraeeni et al., 2012), U ($m \cdot s^{-1}$) can be represented as the wind velocity at 2 m. Previous studies have determined δ based on velocity convections in which a = 3.9 and a = 2.26 were assumed under laminar flow and turbulent flow respectively (Ben Neriah et al., 2014; Haghighi & Or, 2013; Shahraeeni et al., 2012). Parameter a is generally determined through calibration against measured data. The present study selected a=2.06 and a=5.8 for saturated textures and the water surface respectively, to close the measured PE under consideration of monthly sums of PE and diurnal courses of PE. The selection of parameter a in the present study will be introduced in Results section.

The calculations for determining the parameters for Equation (1) and Equation (7) are provided in the Appendix [Appendix Equations (A1–A7)].

3. Results

3.1 Meteorological condition of the research area

Figure 2 shows the average diurnal cycles of meteorological elements across different seasons during the study period.

Meteorological variables typically showed diurnal cycles. The peak yearly T_a occurred in summer due to higher incoming radiation, whereas the coldest days occurred between December and January. The peak T_a lagged the R_n due to thermal inertia of the air. Relative humidity (RH) showed an inverse relationship to T_a. Wind speed showed a clear diurnal cycle with higher value during the day and lower value at night. The study area generally showed a relatively low wind speed. Consistent with Equation (A7), the pattern within the vapor pressure (e_a) curve differed

from those of other meteorological variables, with a peak in the mid-morning, besides for in winter during which the peak occurred in the late morning. Net radiation ($W \cdot m^{-2}$) curves are in bell-shape, R_n peaks around 12:40 (Beijing time). Since there was virtually no incoming shortwave radiation at night, the negative R_n could be mainly attributed to upward longwave emissivity.

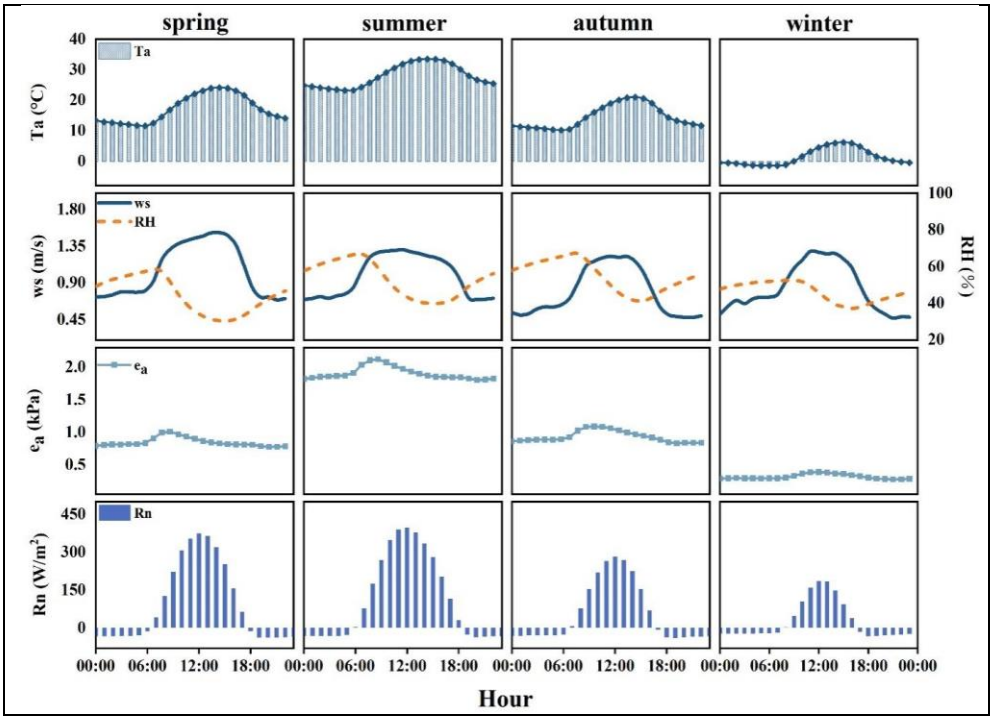

Figure 2: Average diurnal cycles of air temperature, wind speed, relative humidity, actual vapor pressure, and net radiation in different seasons.

3.2 Measured PE over saturated bare soils and water

Cumulative evaporation from two saturated sandy soils, water, and Class A Pan over the study period are plotted in Figure 3. There were clear differences in PE among the different surfaces with increasing cumulative evaporation. The maximum and minimum PE were observed for fine sand and water, respectively. PE_{fine} exceeded PE_{col}, PE_{pan}, and PE_{coarse} by 12.6%, 13.1%, and 7.3%, respectively during the measurement period. These differences were more pronounced in summer. For example, from June to August, PE_{fine} exceeded PE_{col}, PE_{pan}, and PE_{coarse} by 15.1%, 11.9%, and 9.4%, respectively. The measured cumulative evaporation curves were parallel to each other from September until the end of November, indicating only

minor differences in PE among different surfaces in autumn). The duration of the frost period (daily minimum temperature below 0 ℃) from December to January was 68 days. The frozen conditions in winter effectively prevented any increase in cumulative evaporation.

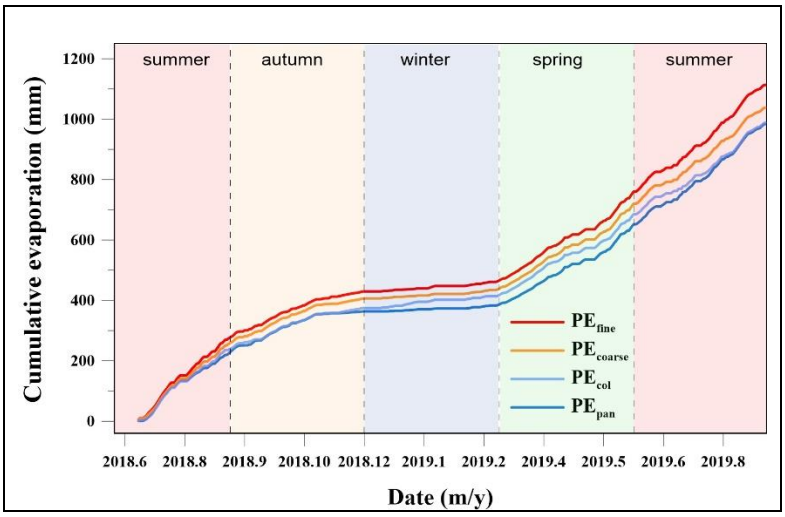

Figure 3 Cumulative evaporation over saturated fine sand, coarse sand, water, and Class A Pan water over the study period

The cumulative PE for spring, summer, and autumn was basically equal to that for the year in the study period. The present study selected March, August, and October as months representative of spring, summer, and autumn, respectively, and conducted detailed analyses for these three months. Figure 4 shows the measured average diurnal PE for saturated fine sand, coarse sand, water, and Class A Pan water over the three seasons.

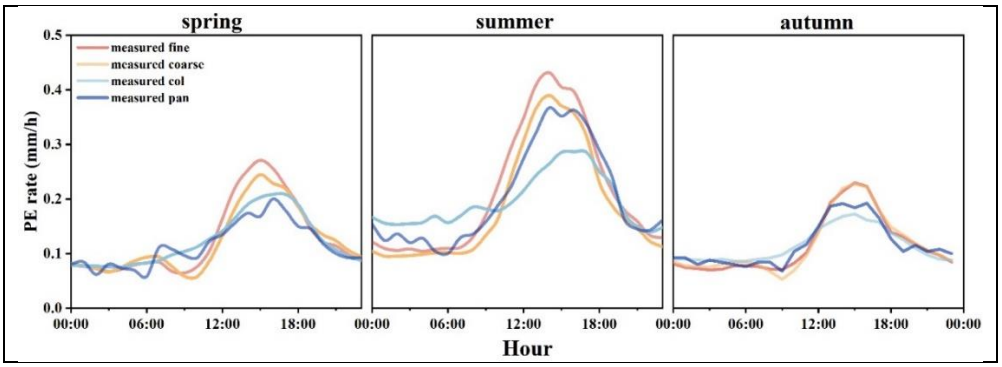

Figure 4 Measured diurnal potential evaporation (PE) curves for saturated fine sand, coarse sand, water in column, and water in Class A Pan over different seasons.

There was a daily peak in the diurnal PE cycles of saturated soils in the afternoon. In spring and autumn, there is another “small PE peak” exists after sunrise. The effect of soil texture on

PE was more obvious under a high evaporation demand, such as during the daytime in spring and summer. Moreover, the observations showed considerable nighttime PE_s and an average nighttime PE over the two saturated sandy soils exceeding 1.0 mm/day in spring and summer. Specifically, PE showed diurnal variation, decreasing after sunset and stabilizing until the second part of the night (Figure 4).

There were absolute and temporal differences in the diurnal dynamics of PE_s and PE_w curves (Li et al., 2020). The cumulative daily PE_s exceeded that of PE_w, with $PE_s > PE_w$ before noon till the sunset, and $PE_s < PE_w$ before dawn until morning. As shown in Figure 4, ~66% of the cumulative daily PE_s occurred between sunrise and sunset in August, with the reminding 34% occurring at night. Nighttime evaporation from soil was ~32% smaller than that during the day. For water, nighttime evaporation is only ~10% smaller than daytime evaporation. In addition, the peak values of PE_{fine} and PE_{coarse} exceeded that of PE_{col}, and occurred at ~14:00 for saturated sandy soils, whereas the peak PE_{col} (~17:00) lagged ~4 h behind that in PE_s.

The results also showed that Class A Pan evaporation approximated the evaporation in the deeper lysimeter column on a yearly scale. At a sub-daily scale, PE_{pan} exceeded PE_{col} after noon but was less than PE_{col} at night. The temporal dynamics of the PE_{pan} curve were similar to those of the PE curves for saturated bare soils. The measured PE_{pan} curve showed fluctuations, particularly under a smaller evaporation demand (such as between sunset and sunrise). This result could be attributed to accuracy of the Class A Pan evaporation gauge is 0.1mm, water level variation smaller than 0.1mm cannot be captured.

3.3 Temperature variations over different evaporation surfaces

Figure 5 shows the average diurnal temperature variations for saturated fine sand (T_{fine}), coarse sand (T_{coarse}), water in the column (T_{col}) and water in the Class A Pan (T_{pan}) in different seasons.

There were slight differences in surface temperature among the saturated sandy soils. The variation in surface temperature of coarse sand exceeded that for fine sand due to its smaller heat capacity. Different to that for saturated textures and Pan water, the surface temperature of water

in the column is the lowest at noon, but highest around the dusk.

There were considerable differences in temperature distributions with depth among soil and water. Surfaces with saturated textures showed a delayed downward heat transport compared to those of other surfaces. As shown in Figure 5, the delay was indicated by an angle, with slower transmission associated with larger angles. Temperature discretization in water was not as obvious as that in soil, resulting in a smaller angle in the water column than in saturated textures. Since T_{col} is relatively uniform in summer, the gradient angle along the vertical profile in summer approximated 0 (Figure 5). In particular, shallow Pan water was well mixed with a vertically homogenous temperature and angle of 0 over the different seasons.

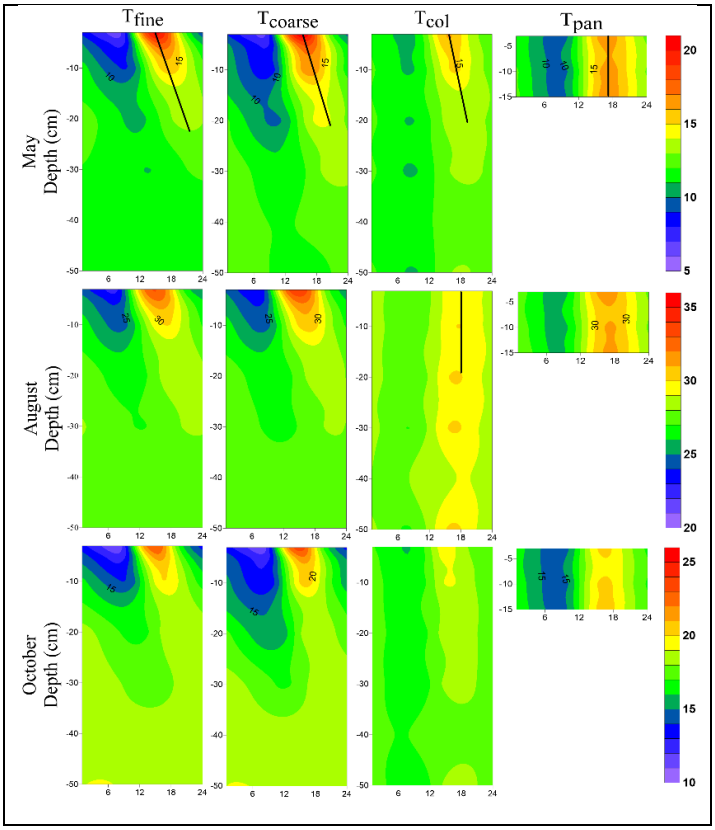

Figure 5 Variations in average diurnal temperature in the soil columns, water column, and water in Class A Pan over different season during the study period and in the study area.

The temperature dynamics observed in the results could be attributed to: (1) a smaller heat capacity resulting in more obvious variations in soil temperature; (2) higher heat capacity enhancing water convection, eventually resulting in a more homogeneous vertical temperature in water; (3) penetration of the water by shortwave radiation, resulting in warming of a larger

vertical column compared to that in soil (incoming radiation does not penetrate soil profile, resulting in heating of only the soil surface).

3.4 Energy balance components

Figure 6 shows the average diurnal cycles of energy flux terms [in Equation (1)] over saturated fine sand, coarse sand, water in the column, and Pan water over different seasons.

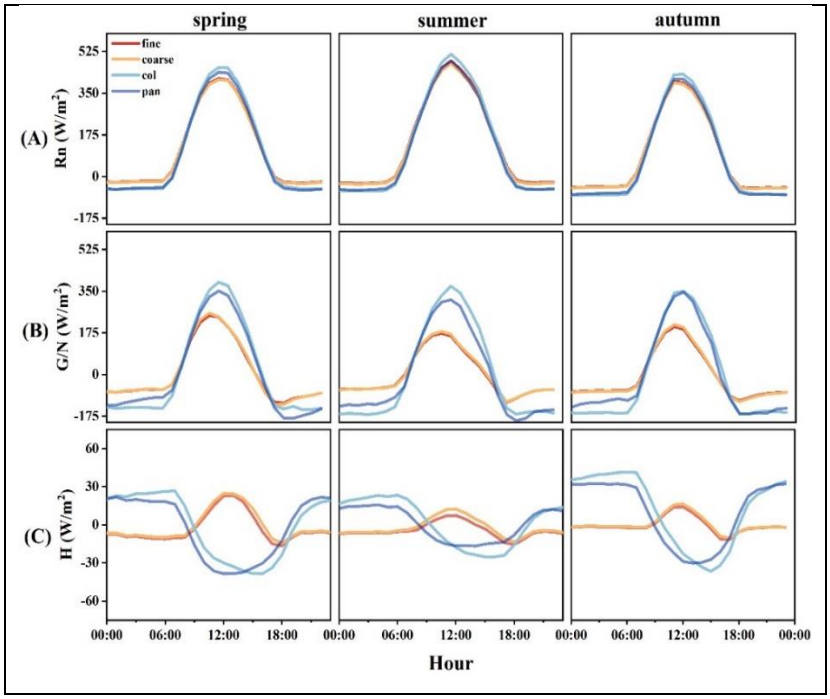

Figure 6 Average diurnal cycles of energy fluxes of the energy balance equation for saturated fine sand, coarse sand, water in column and water in Class A Pan over different seasons: net radiation (A), heat flux/heat storage variation (B), sensible heat flux (C).

3.4.1 Net radiation

As shown in Figure 6A, R_n was slightly negative at night, following which it increased to a positive value after sunrise (summer: between 5:00 and 6:00, spring and autumn: between 6:00 and 7:00). The value of R_n exceeded those of other flux terms and was influenced by albedo (which affects net shortwave radiation R_{ns}) and surface temperature (which affects upward longwave radiation R_{lu}). Based on our measurements, coarse sand is slightly higher in albedo (Appendix Table , which results in smaller R_{ns}) and surface temperature (which enhances the outgoing longwave radiation R_{lu}) than fine sand. Consequently, R_n for coarse is slightly smaller

than fine sand both during the day and at night. Furthermore, a weaker variation in surface temperature for column water (Figure 5) resulted a smaller R_{lu} and a more obvious change in R_n compared to that of saturated textures and Pan water.

3.4.2 Heat flux and heat storage variation

Total ground heat flux G and the variation in water heat storage N represent the below-surface redistribution of energy. The values of G and N were highly related to variations in temperature along depths and surface thermal properties. Figure 6B shows the average diurnal cycles of G and N for different surfaces over different seasons.

According to Equation (5), N is determined by temporal temperature variations T_i-T_{i-1} and water depth Δz. Under a vertically homogenous temperature (for example in summer), the amplitude of N_{col} for the deeper column exceeds that of N_{pan} due to its larger depth (Figure 6B). While, N_{col} and N_{pan} did not show significant differences during daytime in autumn. This is because more pronounced temperature variations (T_i-T_{i-1}) in Pan will compensate the influence of smaller Δz for the Class A Pan. As for soils, G_{coarse} has bigger amplitude than G_{fine}. This is related to a more pronounced temperature variation of the coarse sand. N for water have a particularly evident amplitude than G. This is related to the increased heat capacity of water compared to the soil.

N and G also showed differences in temporal dynamics. Both N and G turned from negative to positive simultaneously in the morning with increasing solar radiation, G peaked in the late morning, whereas N showed an obvious lag response to G (Figure 6B). Both G and N were positive in the day and negative at night, indicating storage of energy under the surface during the day and its release at night.

On seasonal basis, the amplitudes of G and N in spring and autumn exceeded those in summer, which could be attributed to a stronger heating-cooling process (which results in higher temperature gradients shown in Figure 5) below the evaporation surface throughout these two seasons. Over longer time scales, the positive values of G and N in spring and summer allowed

the storage of heat, whereas their negative values in autumn and winter allowed this stored heat to dissipate.

3.4.3 Sensible heat flux

Figure 6C shows the average diurnal cycles of *H* for different surfaces among the different seasons. Daytime (9:00 to 15:00) soil *H* was positive since heat was transferred from soil to air, whereas *H* was negative during the night as heat was transferred from the atmosphere to the soil surface. In contrast, *H* of water was negative during the day (10:00 to 19:00) and positive at night. These opposite trends in nighttime *H* between soil and water were regulated by surface temperature. Generally, the absolute value of *H* over well-watered surface is the smallest among major fluxes in Equation (1) (Finch, 2001; Gallego-Elvira et al., 2011).

3.5 Vapor transfer components

Following Equation (7), PE through vapor diffusion is influenced by wind speed (Figure 7A) and air temperature (Figure 7B). In particular, PE was mostly driven by vapor gradients $e_s(T)/T\text{-}e_a(T_a)/T_a$ (abbreviated to "Δe") between the evaporation surface and the thin layer of air above the surface (Figure 7C).

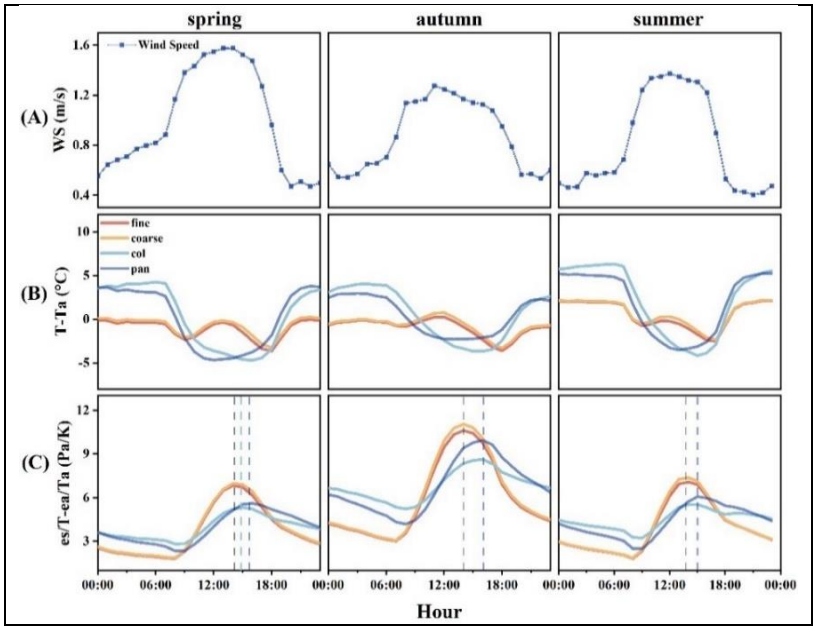

Figure 7 Average diurnal cycles of: (A) wind speed, (B) deficits between surface temperature and air temperature, and (C) vertical vapor gradients (Δe) between different evaporation surfaces and air over different seasons

The average diurnal cycles of Δe above the evaporation surface showed strong correlations with surface temperature, relative humidity, and air temperature. As shown in Figure 7C, the variations of Δe in spring and autumn were moderate compared to those in summer. Over sub-daily scale Δe for saturated sands showed a more pronounced amplitude compared to that for water, and it also peaked before that of water. Δe of Pan water showed a more pronounced amplitude than that of deeper column water. The water column Δe peaked before that of Pan over all seasons, except for summer.

PE through vapor diffusion is also influenced by the boundary layer thickness δ. Following Equation (8), the optimization on parameter a is important for the performance of the vapor transfer equation. Compared with water, a was supposed to have more uncertainty for soil texture. This is because vapor transport from wet porous across the viscous boundary layer will exhibit more complex dynamics compared with smooth free water surface. We changed a series of a to obtain better match between measured and calculated PE for saturated textures. Results are plotted in Figure 10.

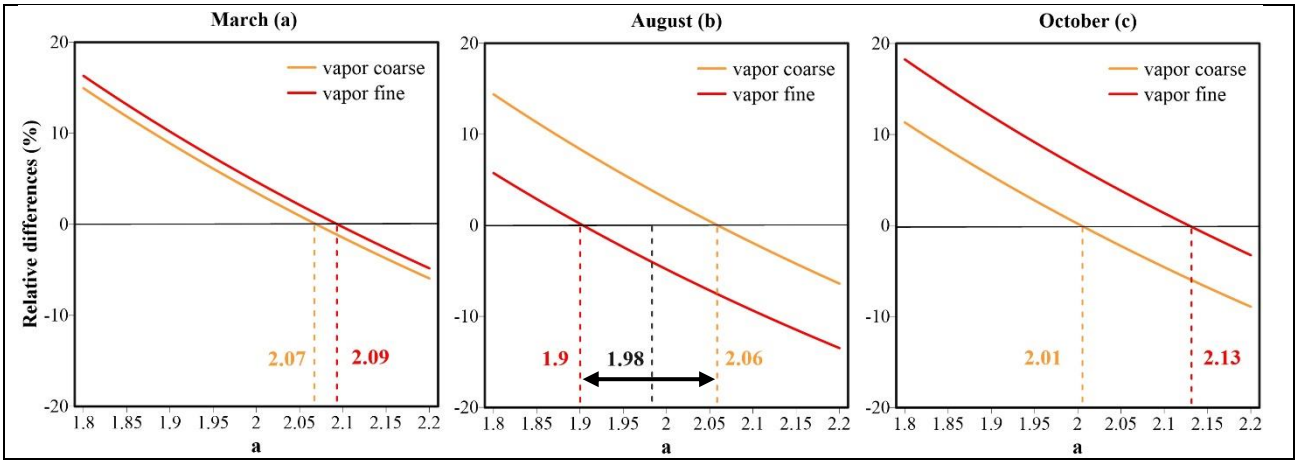

Figure 8 Influence of parameter a on relative differences between calculated and measured PE for saturated fine sand (red solid curve) and coarse sand (orange solid curve) in different seasons.

The relatively larger contribution of PE during summer to the yearly PE demonstrate the importance of PE in hot period. As a result, we constitute a calibration procedure (by modifying a) to close the measured evaporation rate in summer seasons. Relative differences on monthly PE approximate zero when a=1.9 (red solid curve) and a=2.06 (orange solid curve) were

employed for saturated fine sand and coarse sand respectively in August (Figure 8B). 1.9, 2.06, their average 1.98 as well as 2.2 were selected to calculate PE according to the vapor transfer equation. Relative differences between calculated and measured PE for each of the months and for each of the soil textures were plotted in Figure 9. Average value of the absolute relative differences $\overline{ARD}$ (%) between calculated and measured monthly PE for soils were conducted to evaluate the performance of *a*.

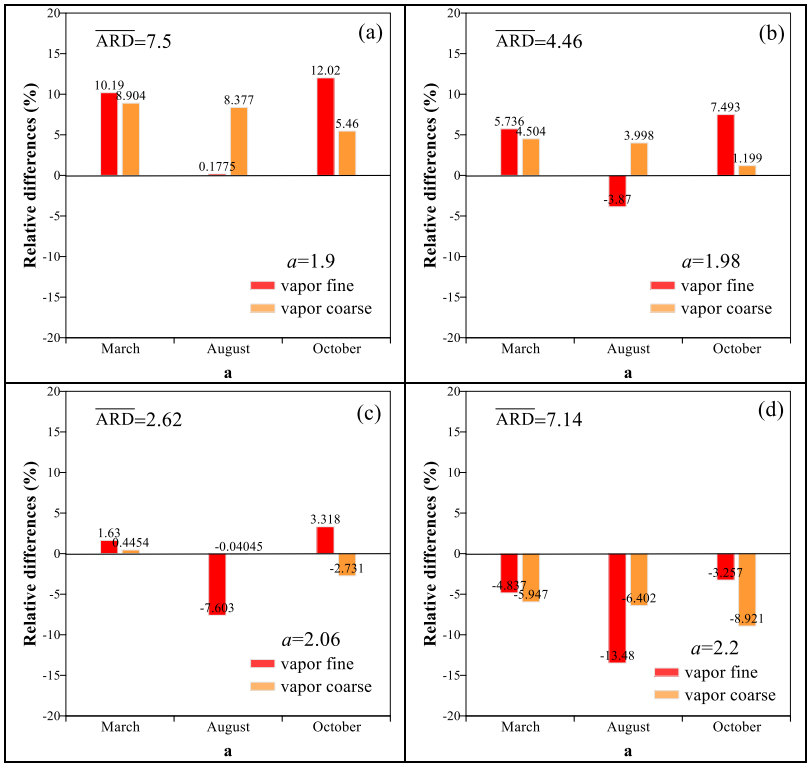

Figure 9 Relative differences between calculated (according to the vapor transfer equation) and measured PE for saturated fine sand and coarse sand in March, August and October.
(a) a= 1.9, (b) a= 1.98, (c) a= 2.06, (d) a= 2.2

Besides the total PE, the optimization on *a* also needs to consider its applicability in estimating diurnal PE dynamics. The influence of *a* on PE dynamics were evaluated as well. Measured and calculated average diurnal PE curves for saturated textures in different seasons were plotted in Figure B1 and Figure B2 (Appendix B). Evaluation statistics results between calculated and measured PE diurnal PE cycles are shown in Table B (Appendix B).

After a exhaustively optimization, we selected a=2.06 for soils since it corresponds the best to the measured total PE (with smallest $\overline{ARD}$, Figure 9b), as well as smaller deviations on

diurnal PE cycles (Table B, a=2.06 provides the smallest MBE, and relatively smaller RMSE) from the measurements (Figure B1 and Figure B2).

As for water in the column and water in Pan, the value of a were modified through trial and error to close the measured PE. We determined that a=5.8 can be recommended for estimating water evaporation.

3.6 Calculated PE

3.6.1 Total PE

Figure 10shows the measured and calculated monthly sums of PE for saturated fine sand, coarse sand, column water, and Class A Pan water according to the vapor transfer equation (Figure 10A) and the energy balance equation (Figure 10B). Differences between measured and calculated PE were plotted for each of the month and for each of the surface in Figure 10C and Figure 10D.

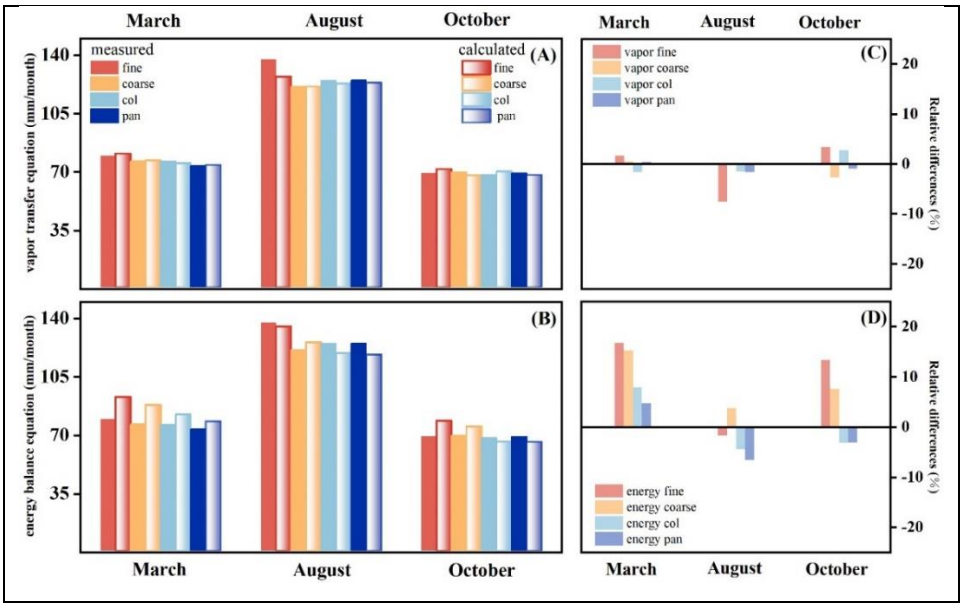

Figure 10 Monthly sums of measured and calculated PE according to the vapor transfer equation (A), the energy balance equation (B). Relative differences between calculated and measured PE sums according to: (C) the vapor transfer equation, (D) the energy balance equation. Results are given for saturated fine sand, coarse sand, water, and water in Class A Pan.

Figure 10C illustrates that, results by the vapor transfer equation showed minor relative differences between measurement and calculation. This method showed the closest match to

observed total PE_{col} and PE_{Pan} in different seasons, but slightly underestimated PE_{fine} when the evaporative demand was high (in August). Figure 10D indicates that the energy balance method overestimated soil evaporations in most seasons but underestimated water evaporations in August and October. Figure 10C and Figure 10D indicate that, the absolute values of relative differences by the vapor transfer method were smaller than by the energy balance method.

3.6.2 Diurnal variations of PE

The comparison of measured and calculated seasonal-specific diurnal PE cycles over different surfaces are plotted in Figure 11 to evaluate the applicability of the vapor transfer equation and energy balance equation on sub-daily scale,

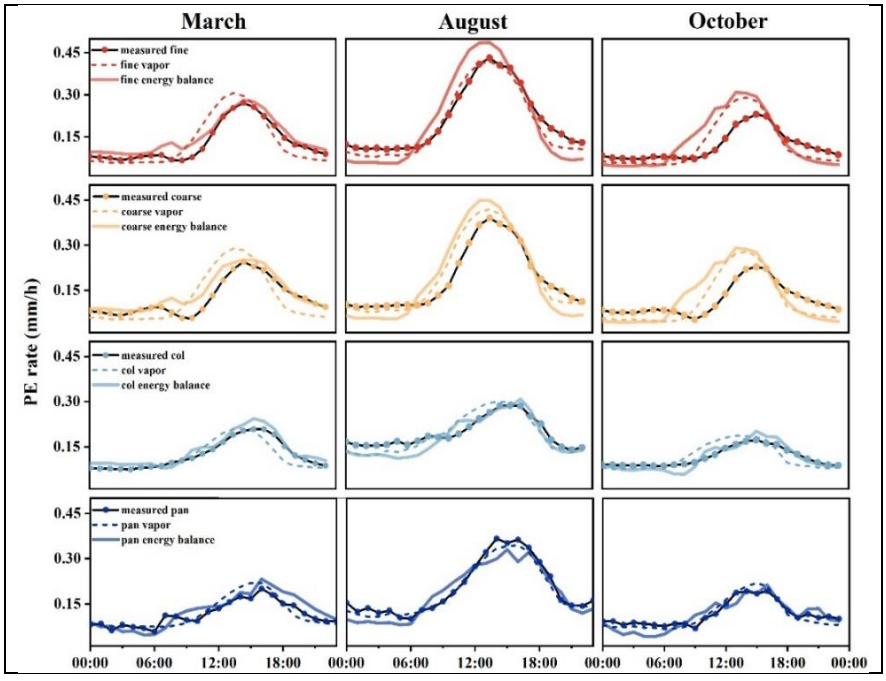

Figure 11 Measured and calculated average diurnal PE curves from saturated fine sand, coarse sand, water in column and water in Class A Pan in different seasons.

A statistical evaluation of the fit between calculated and measured results (Figure 11;

Table) indicates that. Both methods can describe the diurnal PE cycles, but they all resulted in relatively larger errors in estimating PE_s. The vapor transfer method appears to provide a reliable estimation of PE for both soil and water, particularly at night. With calculated results

deviate less from measured data (with smaller RMSE, and MBE in most conditions). However, this method predicts PE_{col}-peak too early in spring and autumn compared with measured results.

The energy balance method resulted in relatively larger deviations from measurements. This energy-unclosure seems to be caused by *G* (for soil) or *N* (for water). The measurements and calculations of *G* or *N* are generally subject to relatively larger uncertainties (Hamdani et al., 2018; Lensky et al., 2018). It should be noted that the energy balance method has advantages in estimating temporal PE dynamics by reproducing the time lag of the evaporation peak over soil and water in spring, as well as reproducing the evaporation peak over water surfaces.

Table 1 Root mean square error (RMSE) and mean bias error (MBE) between calculated and measured evaporation rate (mm/h) for the saturated fine sand, coarse sand, water in column and water in Class A Pan, by the vapor transfer equation and energy balance method for season-specific average diurnal cycles

Evaluation statistics	Method	March				August				October			
		fine	coarse	water	pan	fine	coarse	water	pan	fine	coarse	water	pan
RMSE	vapor	0.04	0.05	0.022	**0.021**	**0.027**	**0.033**	**0.026**	**0.033**	**0.048**	**0.005**	0.023	0.026
	energy	**0.026**	**0.027**	**0.017**	0.025	0.063	0.062	0.029	0.035	0.065	0.065	**0.017**	**0.024**
MBE	vapor	**0.002**	**0.001**	**-0.005**	**0.003**	-0.015	**0.001**	**-0.003**	**-0.01**	**0.005**	**-0.002**	**0.001**	**-0.004**
	energy	0.022	0.019	0.008	0.011	**-0.003**	0.007	-0.014	-0.017	0.016	0.01	-0.003	-0.005

4. Discussion

4.1 Energy transfer in evaporation process

4.1.1 Energy transfer during daytime

The absolute value of *H* over a well-watered surface was the smallest among the flux terms. Energy considerations indicated that the differences in PE between over-saturated soils and water were mostly driven by available energy (R_n-*G* or R_n-*N*).

Albedo determines incoming shortwave radiation. The albedo of soil is mainly influenced by water content and the color of the surface. In this research, the albedo for the coarse sand is slightly higher than fine sand due to the lower porosity and a slightly different color. Albedo of water in the lysimeter column was slightly smaller than those of saturated soil textures since radiation can penetrate deeper below the water column. In general, the higher albedo of water in shallow Class A Pan water could be attributed to some of the received radiation being reflected by the bottom of Pan. Most importantly, surface temperature (*T*) will influence the outgoing

longwave radiation. Overall, as shown in Figure 6, the results showed the ranking of different surfaces according to daytime net radiative flux to be: $R_{n,\,col} > R_{n,\,pan} > R_{n,\,fine} > R_{n,\,coarse}$.

A smaller amount of absorbed R_n does not imply that PE for saturated soil is smaller. The energy re-distribution of the underlying material, which is determined by temperature variations and thermal properties, identified significant differences between saturated soils (G) and water (N). R_n cannot penetrate the soil during the day, and the delay in heat transfer through porous media with depth results in a smaller ground heat flux G (compared with N, Figure 6). Therefore, a significant portion of R_n was converted to evaporation over saturated soil surfaces. In particular, daytime energy available for evaporation over fine sand exceeded that for coarse sand as measurements showed that $R_{n,fine}$-$G_{0,fine} > R_{n,coarse}$-$G_{0,coarse}$ during the day. In addition, the small peak in PE_s at around sunrise could be attributed to the temporal dynamics of available energy. The point at which G changed from negative to positive in spring and autumn lagged behind that of R_n. This delay increased the latent heat flux due to the large deficits between R_n-G (Li et al., 2022).

As for water, a significant portion of R_n was used to heat the deeper column water due to the water having the highest heat capacity. This resulted in less energy available for the latent heat flux ($R_{n,w}$-$N < R_{n,s}$-G) and a delay in the release of stored energy to the latent heat flux and sensible heat flux in water. As a result, the PE_w curves lagged behind PE_s. This time lag was relatively shorter for PE_{pan} since shallow water bodies showed a reduced stored energy N.

4.1.2 Energy transfer at nighttime

Except for water availability, nocturnal water loss achieved the highest positive correlation with wind speed, vapor pressure deficit, downward longwave radiation and a strong negative with relative humidity (Groh et al., 2019; K. E. Skaggs & S. Irmak, 2011; Maheu et al., 2014; Novick et al., 2009; Padrón et al., 2020). Light wind speed and high air relative humidity will inhibit evaporation as water vapor concentration gradient between soil (or water) and air will be too low to reach the latent heat status (Monteith, 1956; Jia et al., 2019). Under this climate condition, nighttime evaporation barely occurred and can be neglected.

Measured results imply that PE from wet surface is considerable and not constant at night., Given the lack of incoming shortwave radiation at night, nighttime G and N were negative due to the release of heat by underlying material stored during the day. Released energy was mainly transferred to the latent heat flux and upward longwave radiation emitted by the evaporation surface. N has more negative value than G at night, as a result, PE_w is higher than PE_s in this period (with $R_{n,w}$-N > $R_{n,s}$-G). On the other hand, there were gradual increases in both G and N (from more negative to less negative) after sunset, leading to a decrease in PE from sunset to dawn. Compared with measured results, nighttime PE is underestimated by the energy balance method (Figure 11). This is because vapor diffusion process also an important contribution to evaporation at night).

4.2 Vapor transfer in evaporation process

Figure 12 illustrates the measured PE rates versus wind speed, air temperature, differences between surface temperature and air temperature (T-T_a), and vertical vapor gradients (Δe).

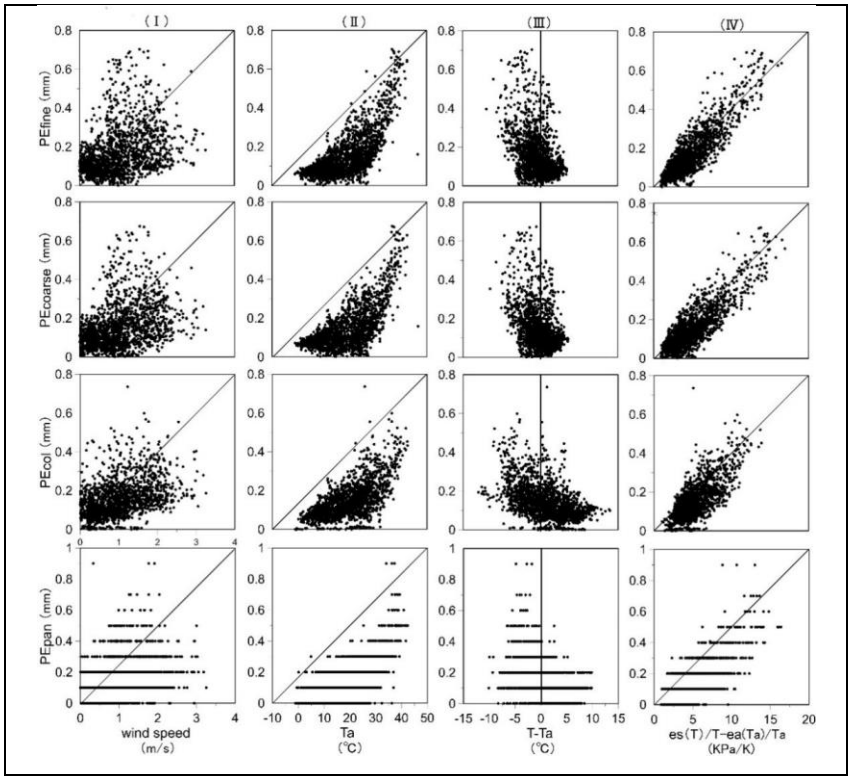

Figure 12 Measured evaporation rates of saturated fine sand, coarse sand, and water vs. wind speed (I), air temperature (II), differences between surface temperature and air temperature (III), and vertical vapor gradients (IV).

The observations suggest that high wind speed and air temperature T_a enhance PE (Figure 12I, Figure 12II). While wind speed has a more erratic pattern than T_a.

The deficits between surface temperature and air temperature (T-T_a) indicating thermal stability of the air above the evaporation surface (T-T_a < 0 represents a stable condition) (Hamdani et al., 2018). T-T_a > 0 will result in increased mixing convection, and this unstable thermal condition generally enhances the evaporation rate under most conditions due to vapor transfer. However, the results shown in Figure 10III imply that PE was not directly proportional to thermal instability. The PE peaks for both water and saturated textures occurred mostly under stable conditions (when T-T_a < 0).

Fick's first law of diffusion stipulates that vapor transfer during the evaporation process follows the "*vapor gradients (*Δe*)"* pattern (Hamdani et al., 2018). The measured PE cycles mostly followed those of Δe. While peaks in PE calculated by Equation (7) were not always aligned with measured peaks (Figure 11, Figure 12) since the vapor diffusion equation does not consider the complex energy transfer process below the evaporation surface.

The good performance of the vapor transfer equation achieved in the present study was highly dependent on the selection of suitable values of parameters a for saturated soil and water [in Equation (8)]. The present study ensured the same environmental conditions across the saturated sands and water. Lysimeter columns and Class A Pan are cylindrical with same area. Calibration results showed that the parameter a differed between saturated soil and water. This difference could be attributed to the relationships of δ with airflow as well as with the characteristic length of the evaporating surface according to boundary layer theory (Haghighi & Or, 2013; Lim et al., 2012). In other words, the thickness of the boundary layer δ in the vapor diffusion equation should be carefully considered instead of defined δ only as a function of stream velocity.

4.3 Evaluation of PE estimation methods: the controlling factors

546 The results of the present study indicated that the energy balance method showed
547 advantages for estimating PE dynamics. This method is recommended for applications which
548 require a high temporal resolution of PE dynamics, such as for precision agriculture. Given
549 energy considerations and the results of the present study, we concluded that differences in PE
550 and temporal dynamics between saturated bare soils and water are mostly driven by albedo and
551 thermal properties (which influence G and N by influencing the surface temperature and
552 temperature variations along depth). The results of the present study suggest that G and N are
553 important factors explaining differences in total PE and diurnal dynamics in PE between over-
554 saturated soil and water. Therefore, these factors should be comprehensively considered instead
555 of ignored or simplified.
556 Moreover, the vapor diffusion equation can provide reliable estimates of nighttime PE and
557 this method is recommended for estimating evaporation from the water surface. Compared with
558 the energy balance equation, the vapor transfer equation provides a simpler approach. It requires
559 common meteorological variables, surface temperature (which determines Δe) as well as
560 calibration of the boundary layer thickness δ against historical evaporation data. In this research,
561 choosing different a for saturated soils and water constitutes a simple calibration procedure to
562 close the measured evaporation rate. A more comprehensive analysis of the influence of seasonal
563 dynamics on a was beyond the scope of this paper and will be considered in future works.
564 Finally, previous research considered surface temperature T to be an independent external
565 forcing that determine "wet surface" evaporation (Tu et al., 2021; Yang & Roderick, 2019). The
566 results of the present study suggest that T is a significant internal forcing for both energy and
567 vapor transfer during the evaporation process since it influences the redistribution of energy
568 below the evaporation surface (G and N), outgoing longwave radiation (R_{lu}), as well as vapor
569 gradients above the surface (Δe).
570
571 **5. Conclusions**
572 The present study conducted high-resolution measurements of evaporation over saturated
573 fine sand (PE_{fine}), coarse sand (PE_{coarse}), and water (PE_{col}) using Markov-Bottle based lysimeters

and Class A Pan evaporation (PE_{pan}) over more than a year. Measured results were comprehensively analyzed using the energy balance method and the improved vapor transfer equation. The following conclusions were derived from the results:

1. There were significant differences in evaporation among the different saturated bare soils and water PE_s is ~12 % higher than PE_w on a yearly scale. There were differences in both absolute values and temporal dynamics of diurnal PE curves between saturated soils and water. Annual PE_{fine} exceeded PE_{coarse} by 7.3%, with the differences more obvious during daytime in spring and summer. The cumulative evaporation over water column and Class A Pan showed minor differences. Compared with PE_{col}-curve, the PE_{pan}-curve resembles more the PE_s-curves over sub-daily scale.

2. Based on energy considerations, we conclude that differences in PE and PE temporal dynamics between saturated bare soils and water were mostly driven by available energy R_n-G *or* N. The vapor transfer processes over saturated soil and water were governed by different vapor pressure gradients above the surface as well as different boundary layer thicknesses.

3. The energy balance method showed advantages for estimating temporal dynamics in PE by reproducing the time lag of the evaporation peak. Energy transfer over different surfaces is controlled by deficits between albedo (which influences R_{ns}) and surface thermal properties (which influences R_{nl}, G, and N by influencing the variations in surface temperature and soil temperature along depth). This research proposes the precisely determination of G and N over different evaporation surfaces instead of ignoring these processes or their simplified representation as a fixed fraction. The vapor transfer equation is simpler and can reliably estimate PE. The vapor transfer processes over different surfaces were a function of surface temperature (which determines vapor gradients Δe) and boundary layer thickness δ.

Acknowledgements

We thank the editor, associate editor and the anonymous reviewers for their constructive feedback. We want to thank to Zhi Li and Yike Wang for the ongoing maintenance of the experimental setup. This research is supported by the National Nature Science Foundation of China (Nos.U1603243, 41230314, 42130710). Chinese Scholarship Council: Program for Joint Training Ph.D. Student Project. Chang'an University Short-Term Study Abroad Program for Postgraduate Students (300104190103).

References

Allen, R. G., Howell, T. A., Pruitt, W. O., Walter, I. A., & Jensen, M. E. (1991). *Lysimeters for Evapotranspiration and Environmental Measurements*. 456–456. https://cedb.asce.org/CEDBsearch/record.jsp?dockey=0073358

Allen, R. G., Jensen, M. E., Wright, J. L., & Burman, R. D. (1989). Operational estimates of reference evapotranspiration. *Agronomy Journal*, *81*(4), Article 4.

Allen, R. G., Pereira, L. S., Raes, D., & Smith, M. (1998). Crop evapotranspiration-Guidelines for computing crop water requirements-FAO Irrigation and drainage paper 56. *Fao, Rome*, *300*(9), Article 9.

Allen, R. G., Pereira, L. S., Smith, M., Raes, D., & Wright, J. L. (2005). FAO-56 dual crop coefficient method for estimating evaporation from soil and application extensions. *Journal of Irrigation and Drainage Engineering*, *131*(1), Article 1.

Allen, R. G., Pruitt, W. O., & Jensen, M. E. (1991). *Environmental Requirements of Lysimeters*. 170–181. https://cedb.asce.org/CEDBsearch/record.jsp?dockey=0072399

Ben Neriah, A., Assouline, S., Shavit, U., & Weisbrod, N. (2014). Impact of ambient conditions on evaporation from porous media. *Water Resources Research*, *50*(8), 6696–6712. https://doi.org/10.1002/2014WR015523

Bird, R. B., Stewart, W. E., Lightfoot, E. N., & Meredith, R. E. (1961). Transport Phenomena. *Journal of The Electrochemical Society*, *108*(3), 78C. https://doi.org/10.1149/1.2428074

Bormann, H. (2011). Sensitivity analysis of 18 different potential evapotranspiration models to observed climatic change at German climate stations. *Climatic Change*, *104*(3–4), 729–753. https://doi.org/10.1007/s10584-010-9869-7

Cellier, P., Richard, G., & Robin, P. (1996). Partition of sensible heat fluxes into bare soil and the atmosphere. *Agricultural & Forest Meteorology*, *82*(1), Article 1. https://doi.org/10.1016/0168-1923(95)02328-3

Dalton, J. (1802). Experimental essays on the constitution of mixed gases; on the force of steam or vapor from water and other liquids in different temperatures, both in a Torricellian vacuum and in air; on evaporation and on the expansion of gases by heat. *Memoirs of the Literary and Philosophical Society of Manchester*, *5*(2), Article 2.

Eberbach, P. L., Humphreys, E., & Kukal, S. S. (2011). The effect of rice straw mulch on evapotranspiration, transpiration and soil evaporation of irrigated wheat in Punjab, India. *Agricultural Water Management*, *98*(12), Article 12.

Finch, J. W. (2001). A comparison between measured and modelled open water evaporation from a reservoir in south-east England. *Hydrological Processes*, *15*(14), Article 14. https://doi.org/10.1002/hyp.267

Gallego-Elvira, B., Baille, A., Martin-Gorriz, B., Martínez-Alvarez, V., & Maestre-Valero, J. F.

(2011). Energy balance and evaporation loss of an irrigation reservoir equipped with a suspended cover in a semiarid climate (south-eastern Spain). *Hydrological Processes*, *25*(11), Article 11.

Ghezzehei, T. A., Trautz, R. C., Finsterle, S., Cook, P. J., & Ahlers, C. F. (2004). *Modeling Coupled Evaporation and Seepage in Ventilated Tunnels*. 40.

Gianniou, S. K., & Antonopoulos, V. Z. (2007). Evaporation and energy budget in Lake Vegoritis, Greece. *Journal of Hydrology*, *345*(3), Article 3. https://doi.org/10.1016/j.jhydrol.2007.08.007

Goss, M. J., & Ehlers, W. (2010). The role of lysimeters in the development of our understanding of soil water and nutrient dynamics in ecosystems. *Soil Use & Management*, *25*(3), Article 3. https://doi.org/10.1111/j.1475-2743.2009.00230.x

Granger, R. J. (1989). An examination of the concept of potential evaporation. *Journal of Hydrology*, *111*(1–4), 9–19. https://doi.org/10.1016/0022-1694(89)90248-5

Griend, A. A. V. D., & Owe, M. (1994). Bare soil surface resistance to evaporation by vapor diffusion under semiarid conditions. *Water Resources Research*, *30*(2), Article 2. https://doi.org/10.1029/93WR02747

Groh, J., Pütz, T., Gerke, H. H., Vanderborght, J., & Vereecken, H. (2019). Quantification and Prediction of Nighttime Evapotranspiration for Two Distinct Grassland Ecosystems. *Water Resources Research*, *55*(4), 2961–2975. https://doi.org/10.1029/2018WR024072

Haghighi, E., & Or, D. (2013). Evaporation from porous surfaces into turbulent airflows: Coupling eddy characteristics with pore scale vapor diffusion. *Water Resources Research*, *49*(12), 8432–8442. https://doi.org/10.1002/2012WR013324

Haghighi, E., Shahraeeni, E., Lehmann, P., & Or, D. (2013). Evaporation rates across a convective air boundary layer are dominated by diffusion: DIFFUSION-DOMINANT EVAPORATION RATES. *Water Resources Research*, *49*(3), 1602–1610. https://doi.org/10.1002/wrcr.20166

Hamdani, I., Assouline, S., Tanny, J., Lensky, I. M., Gertman, I., Mor, Z., & Lensky, N. G. (2018). Seasonal and diurnal evaporation from a deep hypersaline lake: The Dead Sea as a case study. *Journal of Hydrology*, *562*, 155–167. https://doi.org/10.1016/j.jhydrol.2018.04.057

Han, S., Tian, F., & Hu, H. (2014). Positive or negative correlation between actual and potential evaporation? Evaluating using a nonlinear complementary relationship model. *Water Resources Research*, *50*(2), 1322–1336. https://doi.org/10.1002/2013WR014151

Hellwig, D. H. R. (1973). Evaporation of water from sand, 4: The influence of the depth of the water-table and the particle size distribution of the sand. *Journal of Hydrology*, *18*(3–4), 317–327. https://doi.org/10.1016/0022-1694(73)90055-3

Jensen, M. E., Allen, R. G., American Society of Civil Engineers, & Environmental and Water

Resources Institute (U.S.) (Eds.). (2016). *Evaporation, evapotranspiration, and irrigation water requirements* (Second edition). American Society of Civil Engineers.

Jia, J., Yan, W., Chen, X., & Liu, W. (2019). Characteristics of Horizontal Precipitation in Semi-Humid Forestland in Northern China. *Water*, *11*(5), 975. https://doi.org/10.3390/w11050975

K. E. Skaggs & S. Irmak. (2011). Characterization of Nighttime Evapotranspiration and Other Surface Energy Fluxes and Interactions with Microclimatic Variables in Subsurface Drip and Center-Pivot Irrigated Soybean Fields. *Transactions of the ASABE*, *54*(3), 941–952. https://doi.org/10.13031/2013.37119

Kirono, D. G. C., Jones, R. N., & Cleugh, H. A. (2010). Pan-evaporation measurements and Morton-point potential evaporation estimates in Australia: Are their trends the same? *International Journal of Climatology*, *29*(5), Article 5. https://doi.org/10.1002/joc.1731

Labedzki, L. (2011). *Evapotranspiration*. BoD–Books on Demand.

Lawrence, D., Fisher, R., Koven, C., Oleson, K., Swenson, S., Vertenstein, M., Andre, B., Bonan, G., Ghimire, B., & van Kampenhout, L. (2019). *CLM5 documentation*. Tech. rep., Boulder, CO: National Center for Atmospheric Research.

Lehmann, P., Merlin, O., Gentine, P., & Or, D. (2018). Soil Texture Effects on Surface Resistance to Bare-Soil Evaporation. *Geophysical Research Letters*, *45*(19), 10,398-10,405. https://doi.org/10.1029/2018GL078803

Lehmann, P., & Or, D. (2013). Effect of wetness patchiness on evaporation dynamics from drying porous surfaces. *Water Resources Research*, *49*(12), 8250–8262. https://doi.org/10.1002/2013WR013737

Lensky, N., Lensky, I. M., Peretz, A., Gertman, I., Tanny, J., & Assouline, S. (2018). Diurnal course of evaporation from the Dead Sea in summer: A distinct double peak induced by solar radiation and night sea breeze. *Water Resources Research*, *54*(1), Article 1. https://doi.org/10.1002/2017WR021536

Lhomme, J. P., & Guilioni, L. (2010). On the link between potential evaporation and regional evaporation from a CBL perspective. *Theoretical and Applied Climatology*, *101*(1), 143–147. https://doi.org/10.1007/s00704-009-0211-0

Lhomme, J.-P. (1997). Towards a rational definition of potential evaporation. *Hydrology and Earth System Sciences*, *1*(2), 257–264. https://doi.org/10.5194/hess-1-257-1997

Li, W., Brunner, P., Hendricks Franssen, H.-J., Li, Z., Wang, Z., Zhang, Z., & Wang, W. (2020). Potential evaporation dynamics over saturated bare soil and an open water surface. *Journal of Hydrology*, *590*, 125140. https://doi.org/10.1016/j.jhydrol.2020.125140

Li, W., Hendricks Franssen, H.-J., Brunner, P., Li, Z., Wang, Z., Wang, Y., & Wang, W. (2022). The role of soil texture on diurnal and seasonal cycles of potential evaporation over saturated bare soils – Lysimeter studies. *Journal of Hydrology*, *613*, 128194.

https://doi.org/10.1016/j.jhydrol.2022.128194

Lim, W. H., Roderick, M. L., & Farquhar, G. D. (2016). A mathematical model of pan evaporation under steady state conditions. *Journal of Hydrology*, *540*, 641–658. https://doi.org/10.1016/j.jhydrol.2016.06.048

Lim, W. H., Roderick, M. L., Hobbins, M. T., Wong, S. C., & Farquhar, G. D. (2013). The energy balance of a US Class A evaporation pan. *Agricultural and Forest Meteorology*, *182–183*, 314–331. https://doi.org/10.1016/j.agrformet.2013.07.001

Lim, W. H., Roderick, M. L., Hobbins, M. T., Wong, S. C., Groeneveld, P. J., Sun, F., & Farquhar, G. D. (2012). The aerodynamics of pan evaporation. *Agricultural and Forest Meteorology*, *152*, 31–43. https://doi.org/10.1016/j.agrformet.2011.08.006

Maheu, A., Caissie, D., St-Hilaire, A., & El-Jabi, N. (2014). River evaporation and corresponding heat fluxes in forested catchments: RIVER EVAPORATION AND CORRESPONDING HEAT FLUXES IN FORESTED CATCHMENTS. *Hydrological Processes*, *28*(23), 5725–5738. https://doi.org/10.1002/hyp.10071

Monteith, J. L. (1956). Evaporation at night. *Netherlands Journal of Agricultural Science*, *4*(1), Article 1. https://doi.org/10.18174/njas.v4i1.17770

Novick, K. A., Oren, R., Stoy, P. C., Siqueira, M. B. S., & Katul, G. G. (2009). Nocturnal evapotranspiration in eddy-covariance records from three co-located ecosystems in the Southeastern U.S.: Implications for annual fluxes. *Agricultural and Forest Meteorology*, *149*(9), 1491–1504. https://doi.org/10.1016/j.agrformet.2009.04.005

Ochsner, T. E., Sauer, T. J., & Horton, R. (2007). Soil heat storage measurements in energy balance studies. *Agronomy Journal*, *99*(1), Article 1. https://doi.org/10.2134/agronj2005.0103S

Padrón, R. S., Gudmundsson, L., Michel, D., & Seneviratne, S. I. (2020). Terrestrial water loss at night: Global relevance from observations and climate models. *Hydrology and Earth System Sciences*, *24*(2), 793–807. https://doi.org/10.5194/hess-24-793-2020

Pütz, T., Fank, J., & Flury, M. (2018). Lysimeters in vadose zone research. *Vadose Zone Journal*, *17*(1), Article 1. https://doi.org/10.2136/vzj2018.02.0035

Roxy, M. S., Sumithranand, V. B., & Renuka, G. (2014). Soil heat flux and day time surface energy balance closure at astronomical observatory, Thiruvananthapuram, south Kerala. *Journal of Earth System Science*, *123*(4), Article 4. https://doi.org/10.1007/s12040-014-0437-9

Saito, H., Sˇimunek, J., & Mohanty, B. P. (2006). Numerical analysis of coupled water, vapor, and heat transport in the vadose zone. *Vadose Zone Journal*, *5*(2), 784–800. https://doi.org/10.2136/vzj2006.0007

Schlünder, E.-U. (1988). On the mechanism of the constant drying rate period and its relevance to diffusion controlled catalytic gas phase reactions. *Chemical Engineering Science*,

753 *43*(10), 2685–2688. https://doi.org/10.1016/0009-2509(88)80012-5
754 Shahraeeni, E., Lehmann, P., & Or, D. (2012). Coupling of evaporative fluxes from drying
755 porous surfaces with air boundary layer: Characteristics of evaporation from discrete pores.
756 *Water Resources Research*, *48*(9). https://doi.org/10.1029/2012WR011857
757 Shuttleworth, W. J. (1993). *Evaporation, Handbook of Hydrology, edited by: Maidment, DR*.
758 McGraw-Hill, New York.
759 Simunek, J., Van Genuchten, M. T., & Sejna, M. (2005). The HYDRUS-1D software package
760 for simulating the one-dimensional movement of water, heat, and multiple solutes in
761 variably-saturated media. *University of California-Riverside Research Reports*, *3*, 1–240.
762 Stewart, J. B., Kustas, W. P., Humes, K. S., Nichols, W. D., Moran, M. S., & de Bruin, H. A.
763 (1994). Sensible heat flux-radiometric surface temperature relationship for eight semiarid
764 areas. *Journal of Applied Meteorology*, *33*(9), Article 9. https://doi.org/10.1175/1520-
765 0450(1994)033<1110:SHFRST>2.0.CO;2
766 Truong, N. (2012). *Quantifying Evapotranspiration Through a Sensitivity Study of Climate*
767 *Factors and Water Table Interactions for a Constructed Wetland Mesocosm*. Villanova
768 University.
769 Tu, Z., Yang, Y., & Roderick, M. L. (2021). *Testing a maximum evaporation theory over*
770 *saturated land: Implications for potential evaporation estimation* [Preprint].
771 Hydrometeorology/Modelling approaches. https://doi.org/10.5194/hess-2021-436
772 Wang, K., & Dickinson, R. E. (2012). A review of global terrestrial evapotranspiration:
773 Observation, modeling, climatology, and climatic variability. *Reviews of Geophysics*, *50*(2),
774 Article 2. https://doi.org/10.1029/2011RG000373
775 Wang, L., Han, S., & Tian, F. (2021). Comparison of formulating apparent potential
776 evaporation with pan measurements and Penman methods. *Journal of Hydrology*, *592*,
777 125816. https://doi.org/10.1016/j.jhydrol.2020.125816
778 Westra, S. (2009). *Hydroclimatology: Perspectives and applications by ML Shelton*.
779 Yang, Y., & Roderick, M. L. (2019). Radiation, surface temperature and evaporation over wet
780 surfaces. *Quarterly Journal of the Royal Meteorological Society*, *145*(720), 1118–1129.
781 https://doi.org/10.1002/qj.3481
782 Zhidong, L., Shixiu, Y., & Senchuan, X. (1988). *Soil hydrodynamics*. Tsinghua University
783 Press, Beijing, China.
784 Zotarelli, L., Dukes, M. D., Romero, C. C., Migliaccio, K. W., & Morgan, K. T. (2010). Step by
785 step calculation of the Penman-Monteith Evapotranspiration (FAO-56 Method). *Institute of*
786 *Food and Agricultural Sciences. University of Florida*.
787

Appendix A

In Equation (2), χ is the surface albedo. The value of χ approximates constant when solar zenith angel φ is greater than 40°. χ at noon can be selected to calculate R_{ns}. In this study area, φ at local solar noon is greater than 40° in most days of the year, and φ at solar noon is smaller than 40° in late autumn and winter. In this research, average local solar noon albedo (measured by CNR4 Net Radiometers Kipp&Zonen, Netherlands) for different saturated soil textures over March, August and October were selected, results are shown in Table .

Table A Local solar noon albedo for saturated soil textures

Sand Type	φ＞40°	φ＜40°
fine	0.100	0.101
coarse	0.105	0.104

where 0.1 and 0.14 are the typical albedo for water and Class A pan (Rotstayn et al., 2006; H. Yang & Yang, 2012). ε is the surface emissivity, representing the reflection coefficient of longwave radiation at the surface. For water, ε=0.97 (Gianniou & Antonopoulos, 2007). For soil, ε can be determined by water content on top surface (Jensen et al., 2016):

$$\varepsilon = \min\left(0.9 + 0.18 \cdot \theta_{top};\ 1.0\right) \tag{A1}$$

In Equation (5), saturated soil volumetric heat capacity calculated using the following equation:

$$c_s = c_{vw} \cdot \theta_s + c_{si} \cdot \left(1 - \theta_s\right) \tag{A2}$$

where c_{vw} (4.19MJ/m³K) is the volumetric heat capacity of water, and θ_s is the saturated water content for the specific soil texture (0.39 for fine sand and 0.37 for coarse sand). c_{si} (MJ/m³K) is the dry soil volumetric heat capacity (0.95 for fine sand and 0.92 for coarse sand) measured by TPS 1500 (Hot Disk, Sweden).

In Equation (6), aerodynamic resistance for saturated soil can be calculated as:

$$r_{a,s} = \frac{\left(\ln\frac{z_1 - d}{z_{om}}\right)\left(\ln\frac{z_2 - d}{z_{ov}}\right)}{k^2 \cdot u} \tag{A3}$$

where k (=0.4) is the von Karman constant, u ($m \cdot s^{-1}$) is the wind speed, z_1 (m) and z_2 (m) are the measurement heights of wind speed (2m) and air temperature (1.5m), d (=0) is the displacement height, z_{om} and z_{ov} are surface roughness lengths for momentum flux and heat flux, with values equal to 0.001 for bare soils (Simunek et al., 2005). The aerodynamic resistance for the water surface can be calculated as:

$$r_{a,w} = \frac{4.72\left(\ln\left(\frac{z_1}{z_0}\right)\right)^2}{1+0.536 \cdot u} \quad \text{(A4)}$$

where z_0 with value equal to 0.00137 is the aerodynamic roughness factor for water surface (Shuttleworth, 1993).

In Equation (7), D_v ($m^2 \cdot s^{-1}$) is the diffusion coefficient for water vapor in air (Ben Neriah et al., 2014):

$$D_v = 2.11 \cdot (\frac{T_a + 273.14}{273.14}) \cdot 10^{-5} \quad \text{(A5)}$$

In Equation (A1), e_s is the vapor pressure at surface (Pa), it is assumed to be equivalent to saturated vapor pressure at surface temperature T. Which can be calculated by (Allen et al., 1998; Zotarelli et al., 2010) :

$$e_s(T) = 610.8 \exp(\frac{17.27 \cdot T}{T + 237.14}) \quad \text{(A6)}$$

In Equation (A1), hourly actual vapor pressure e_a (Pa) is given by:

$$e_a\left(T_a\right) = e_s\left(T_a\right) \cdot RH \quad \text{(A7)}$$

RH is the relative humidity from meteorological station.

Appendix B

Measured and calculated average diurnal PE curves (with different *a*) for saturated soil textures in different seasons were plotted in Figure B1 and Figure B2.

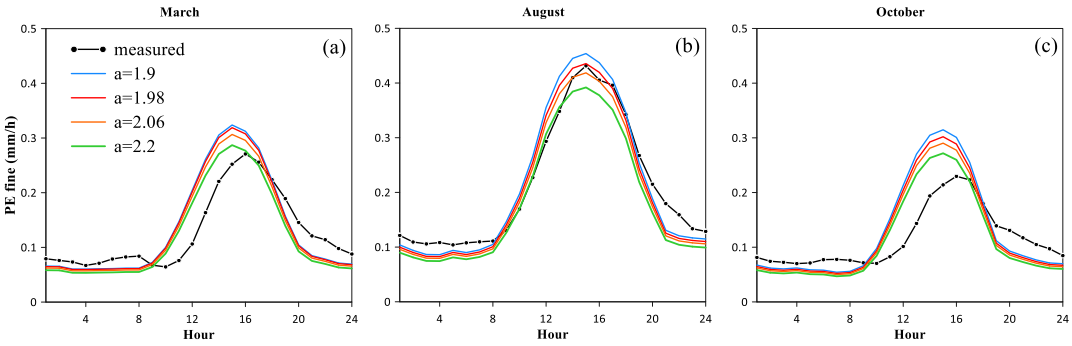

Figure B1 Measured and calculated average diurnal PE curves (by the vapor transfer method, with a= 1.9 in blue, a= 1.98 in red, a= 2.06 in orange, a= 2.2 in green) for saturated fine sand in March (a), August (b) and October (c).

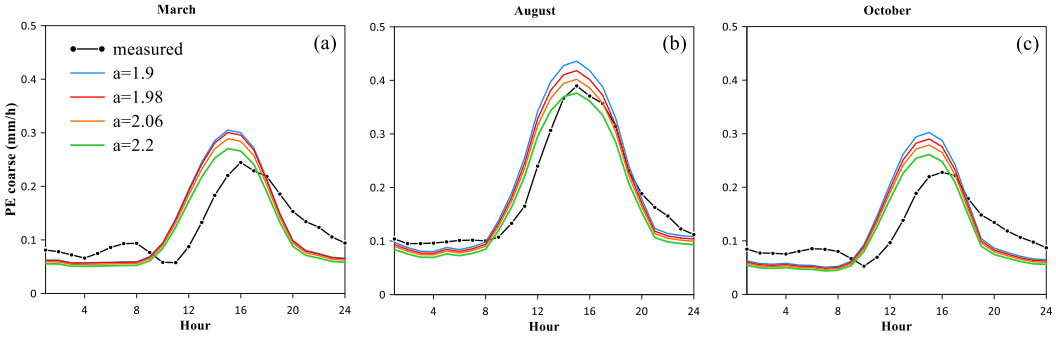

Figure B2 Measured and calculated average diurnal PE curves (by the vapor transfer method, with a=1.9 in blue, a=1.98 in red, a=2.06 in orange, a=2.2 in green) for saturated coarse sand in March (a), August (b) and October (c).

Evaluation statistics between calculated and measured PE for the average diurnal cycles are shown in Table B.

Table B Root mean square error (RMSE) and mean bias error (MBE) between calculated and measured evaporation rate (mm/h) for the saturated fine sand and coarse sand, by the vapor transfer equation for season-specific average diurnal cycles

Evaluation statistics	Soil textures	Average Diurnal PE cycles (mm/h)											
		March				August				October			
		1.9	1.98	2.06	2.2	1.9	1.98	2.06	2.2	1.9	1.98	2.06	2.2
RMSE	fine	0.045	0.043	0.04	**0.037**	0.029	0.027	**0.027**	0.034	0.056	0.052	0.048	**0.042**
	coarse	0.054	0.053	0.05	**0.047**	0.043	0.037	0.033	**0.031**	0.056	0.053	0.05	**0.045**
MBE	fine	0.009	0.007	**0.002**	-0.006	**0.001**	-0.007	**-0.015**	-0.028	0.015	0.01	0.005	**-0.003**
	coarse	0.008	0.006	**0.001**	0.007	0.016	0.008	**0.001**	-0.011	0.008	0.003	**-0.002**	-0.009